Physica B 406 (2011) 3687–3693

Contents lists available at ScienceDirect

Physica B

journal homepage: www.elsevier.com/locate/physb

Photoelectronic characterization of *n*-type silicon wafers using photocarrier radiometry

A. Gutiérrez [a,*], M.E. Rodríguez-García [b], J. Giraldo [a]

[a] Departamento de Física, Universidad Nacional de Colombia-Sede Bogotá, Avenida Carrera 30 No. 45-03, Ciudad Universitaria, Bogotá, DC, Colombia
[b] Centro de Física Aplicada y Tecnología Avanzada, Universidad Nacional Autónoma de México, Campus Juriquilla, Querétaro, Qro. México A.P 1-1010, Mexico

ARTICLE INFO

Article history:
Received 9 April 2010
Received in revised form
22 June 2011
Accepted 29 June 2011
Available online 5 July 2011

Keywords:
Photoelectronic characterization
Photocarrier radiometry
Nondestructive testing
Silicon wafers
Transport properties
Porous silicon

ABSTRACT

Photocarrier radiometry (PCR) was used to characterize four *n*-type silicon wafers with different resistivity values in the 1–20 Ω cm range. Simulations of the PCR signal have been performed to study the influence of the recombination lifetime and front surface recombination velocity on them; besides, the transport parameters (carrier recombination lifetime, diffusion coefficient, and frontal surface recombination) of the wafers were obtained by means of a fitting procedure. The PCR images that are related to the lifetime are presented, and the first photoelectronic images of a porous silicon sample are obtained.

© 2011 Elsevier B.V. All rights reserved.

1. Introduction

The determination of the transport parameters of semiconductors, such as, the carrier recombination lifetime, carrier diffusion coefficient, and front surface recombination velocity, is very important in semiconductor device manufacturing. In the last years, the evaluation of semiconductors by means of photothermal methods has attracted particular attention due to the nondestructive and noncontact character of these techniques. Photocarrier radiometry (PCR) is an example [1–3].

Physically, the signal generation process can be described as follows. Upon impinging on a semiconductor surface, an intensity-modulated laser beam simultaneously produces direct lattice heat due to absorption, as well as a modulation in the free photoexcited carrier density, provided the photon energy is greater than the bandgap energy. If the infrared emissions from the excited region of the sample are filtered and focused onto a narrow-bandwidth infrared detector, such as InGaAs, which has a spectral bandwidth of 0.8–1.8 μm, the signal free of any thermal contribution can be obtained. This photocarrier radiometry (PCR) signal is proportional to the depth integral of the carrier density in the sample [1]:

$$S(\omega) \approx F(\lambda_1,\lambda_2) \int_0^L \Delta N(z,\omega) dz, \quad (1)$$

where L is the simple thickness and $F(\lambda_1, \lambda_2)$ is a coefficient that depends on the spectral bandwidth of the detector $[\lambda_1, \lambda_2]$. $\Delta N(z, \omega)$ is the carrier-wave depth profile, z is the depth starting from the simple wafer front surface, and ω is the angular frequency of the modulation excitation beam.

In this work the PCR technique has been used to characterize photoelectronically *n*-type silicon wafers by means of a 3D PCR model. In Sections 2 and 3 the theoretical effects of the recombination lifetime and the front surface recombination velocity on the shape of the frequency response curves (amplitude and phase) of the PCR signals are presented. In Section 4 various *n*-type silicon wafers are characterized photoelectronically using a theoretical fit of the experimental curves (both amplitude and phase) of the PCR signal; in addition, the photoelectronic images that are related to carrier lifetime are included. Finally, the first photoelectronic images of a porous silicon sample were obtained by means of the PCR technique, as a result these images show that the porous region exhibits a recombination lifetime larger than the substrate.

2. Theoretical model

The semiconductor sample with thickness L is excited by a normally incident Gaussian shaped laser beam with an axially symmetric intensity profile $I=I_o \exp(-r^2/w^2)$, where w is the spotsize of the laser beam. The absorption of superband-gap photons results in a photon density that decays exponentially in

* Corresponding author. Tel.: +571 3165000; fax: +571 3165669.
E-mail address: agutierrezr@unal.edu.co (A. Gutiérrez).

0921-4526/$ - see front matter © 2011 Elsevier B.V. All rights reserved.
doi:10.1016/j.physb.2011.06.073

the axial direction according to $\exp(-\beta z)$, where β is the optical absorption coefficient (the Beer–Lambert law). The semiconductor is assumed thermally and electronically isotropic. The emitted infrared radiation is focused onto an appropriate detector of radius a.

The transport of electronic carriers in a material excited by a modulated source can be described by the temporal Fourier transform of the continuity equation. This equation can be solved in the Hankel space.

The carrier-density-wave field $N(r,z;\omega)$ is the solution of the temporal Fourier transform of the transport equation [4]:

$$\nabla^2 N(r,z;\omega)-\sigma_e^2(\omega)N(r,z;\omega)=-\frac{G_e(r,z;\omega)}{D}, \tag{2}$$

where $\sigma_e^2=(1+i\omega\tau)/D\tau$, τ is the recombination lifetime, and D is the minority carrier diffusion coefficient. The boundary conditions for the carrier-density-wave are

$$D\frac{d}{dz}N(r,z;\omega)\bigg|_{z=0}=S_1N(r,0;\omega), \tag{3a}$$

$$D\frac{d}{dz}N(r,z;\omega)\bigg|_{z=L}=-S_2N(r,L;\omega), \tag{3b}$$

and the injected carrier density is

$$G_e(r,z;\omega)=\frac{\beta P\eta(1-R)}{h\nu\pi w^2}e^{-r^2/w^2}e^{-\beta z}, \tag{4}$$

with S_1 and S_2 the surface recombination velocities on frontal and back surfaces of the sample, P is the power of the incident excitation source, η is the probability that an incident photon produces an electron–hole pair, R is the reflectivity, $h\nu$ is the photon energy, and E_g is the band-gap energy.

The differential Eq. (2) submitted to the boundary conditions (3a and 3b) is resolved by means of the Hankel transform

$$\tilde{F}(q,z;\omega)=\int_0^\infty F(r,z;\omega)J_0(q,r)rdr, \tag{5}$$

and the resulting one-dimensional ordinary differential equation is resolved using Green's function technique [4].

After some algebra, the solution for the carrier-density-wave field in the Hankel space is

$$\begin{aligned}\tilde{N}(q,\omega)&=\int_0^L\tilde{N}(q,z;\omega)dz\\&=E(q)\left[\frac{(1-e^{-\xi_eL})}{\xi_e}(C_1(q)+C_2(q)e^{-\xi_eL})-\frac{(1-e^{-\beta L})}{\beta}\right],\end{aligned} \tag{6}$$

where

$$E(q)=\frac{\beta P\eta(1-R)e^{-q^2w^2/4}}{2h\nu\pi D(\beta^2-\xi_e^2)},$$

$$C_1(q)=A_1A_2\left[\frac{b_1-b_2e^{-(\beta-\xi_e)L}}{A_2-A_1e^{-2\xi_eL}}\right],$$

$$C_2(q)=\frac{b_1A_1-b_2A_2e^{-(\beta-\xi_e)L}}{A_2-A_1e^{-2\xi_eL}},$$

$$A_1\equiv\frac{D\xi_e-S_1}{D\xi_e+S_1},\quad A_2\equiv\frac{D\xi_e+S_2}{D\xi_e-S_2},\quad b_1\equiv\frac{D\beta+S_1}{D\xi_e-S_1},\quad b_2\equiv\frac{D\beta-S_2}{D\xi_e+S_2},$$

$$\xi_e^2=q^2+\sigma_e^2=q^2+\frac{1+i\omega\tau}{D\tau}.$$

Calculation of the radiometric signal due to the carrier-density-wave must take into account the efficiency of the detector by integrating over the effective detector aperture [5]. Assuming a circular aperture of radius a, the PCR signal will be

$$S_{PCR}=\frac{1}{\pi a}\int_0^\infty\tilde{N}(q;\omega)J_1(qa)dq, \tag{7}$$

where $J_1(x)$ is the Bessel function of first kind and order one.

3. Numerical simulations

In order to see the influence of the minority carrier lifetime and the front surface recombination velocity in the PCR signal, the amplitude and phase of the signal were simulated throughout Eq. (7). In calculations, the absorption coefficient of the wafer is assumed as $101.57\times10^4\ \mathrm{m}^{-1}$, which corresponds to the absorption coefficient of the crystalline silicon at 532 nm wavelength [6]. The carrier diffusion coefficient (D) and the back surface recombination velocity (S_2) were taken as $10\ \mathrm{cm}^2/\mathrm{s}$ and 1×10^5 cm/s, respectively; these data correspond to n-type silicon samples according to the values reported by Rodríguez et al. [7]. The thickness of the wafer was taken as 500 μm, the laser spotsize equal to 40 μm and the radius of the detector equal to 40 μm. Table 1 resumes the photoelectronic parameter values used in the simulations.

The theoretical radiometric signal contains improper integrals with infinite upper limits and must be evaluated numerically. Based on the physical quantity represented by the integrand, it is necessary that the integral approaches a finite value as the upper limit of integration approaches infinity. A FORTRAN program was used to perform the integration numerically using the extended trapezoidal rule [8]. The upper limit was replaced by a finite upper limit that was chosen to ensure that any additional contribution due to a further increase in the upper limit was negligible [9]. The program was then used to calculate a theoretical response for a given set of electronic and thermal parameters.

3.1. Recombination lifetime simulations

Fig. 1a and b shows the amplitude and phase of the PCR signal as a function of modulation frequency for different values of the recombination lifetime; on the other hand, in Fig. 1c and d the amplitude and phase of the PCR signal as a function of the lifetime with the modulation frequency as a parameter are plotted. The amplitude and phase dependencies are similar to the ones described previously by Li et al. [10]. The amplitude and phase increase with increasing the carrier lifetime, and become saturated above a certain value of lifetime.

From Fig. 1 it is observed that the amplitude and phase present a slope change starting from a certain critical frequency $f_c\approx1/2\pi\tau$. The amplitude diminishes when the lifetime decreases due to enhanced recombination resulting in decreased excess plasma density. For recombination lifetimes longer than 100 μs the signal phase saturates. For these long-lived plasma waves, the mechanism that governs the phase-shift is the storage of photoexcitation energy in the form of coherently diffusing free-carrier oscillations. As the lifetime increases, a greater fraction of the overall excess

Table 1
Values taken for electronic parameters of n-type silicon wafers for the simulations of the PCR signal. The laser beam size and the detector radius were included.

Parameter	Value
τ (μs)[a]	10
D (cm^2/s)	10
S_1 (cm/s)[b]	300
S_2 (cm/s)	1×10^5
a (μm)	40
w (μm)	40

[a] For the simulations of the PCR signal as a function of S_1 the carrier lifetime was $\tau=10$ μs.

[b] For the simulations of the PCR signal as a function of τ the front surface recombination velocity was $S_1=300$ cm/s.

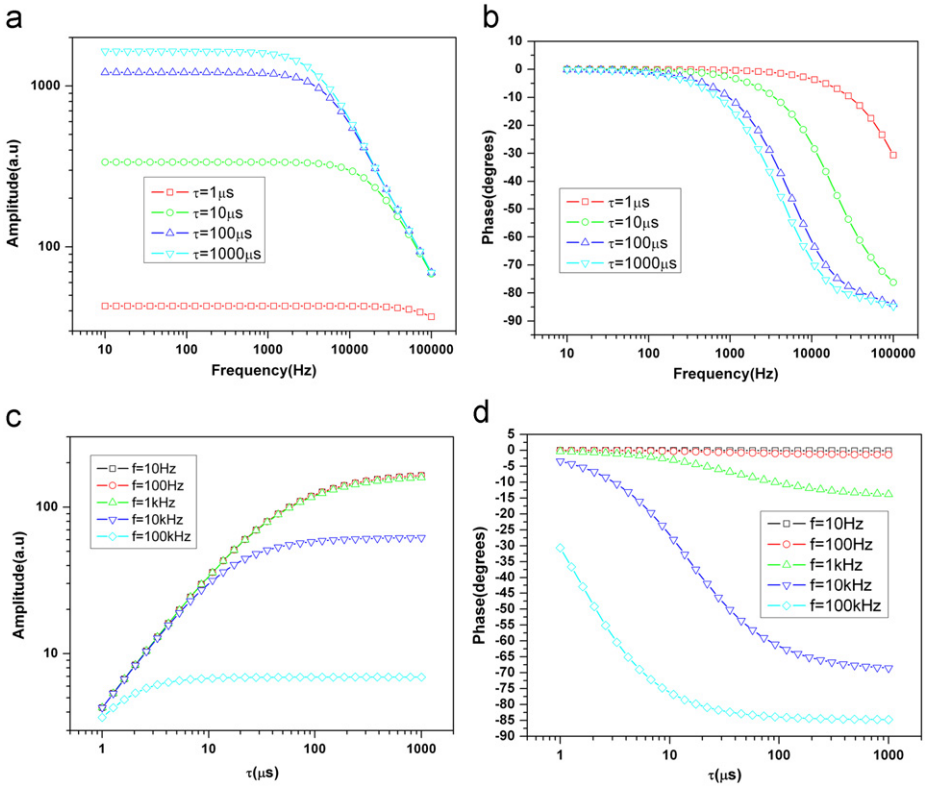

Fig. 1. Simulated PCR signal as a function of the modulation frequency and the carrier lifetime. ((a) and (b) correspond to the amplitude and phase of the signal as a function of the modulation frequency with the recombination lifetime as a parameter. (c) and (d) correspond to the amplitude and phase of the PCR signal as a function of the carrier lifetime with the modulation frequency as a parameter).

density fails to follow the fast decay of the optical waveform since it recombines with a rate proportional to $\tau^{-1} \ll f$. In the limit of long lifetimes, the entire excess carrier-density-wave remains in the free (excited) state during one modulation period and the phase lag saturates at -90° [4].

3.2. Front surface recombination velocity simulations

PCR signal simulations as a function of the front surface recombination velocity of the silicon wafer are plotted in Fig. 2. This phenomenological parameter is a measure of the electronic quality of the front surface in terms of the structure and density of traps and surface states acting as recombination sites [7]. Fig. 2a and b shows a similar behavior to the case observed for the recombination lifetime (Fig. 1a and b): the amplitude and phase exhibit a characteristic bend "knee"; nevertheless, in this case this knee shifts to higher frequencies as the front surface recombination velocity increases. The amplitude and phase are both sensitive to the front surface recombination velocity in the 100–10^4 cm/s range; the amplitude decreases with increasing S_1 meanwhile the phase increases. This behavior is related to the carrier diffusion length.

Although the diffusion length of an excited carrier is related to the diffusion coefficient and the recombination lifetime by means of $L_D=(D\tau)^{1/2}$, for modulated injected carriers the distance traveled by a carrier is described by the diffusion length of the carrier-density-wave, $L_{ac}(f)=(D\tau/(1+i2\pi f\tau))^{1/2}$ [11].

Since the diffusion length L_{ac} diminishes as the frequency increases, the injected carriers remain closer to the surface increasing the interaction probability with the recombination centers. The high recombination rates due to the big values of the front surface recombination diminish the carrier density resulting in lower amplitudes and higher phases.

For values of S_1 below 100 cm/s and over 10^4 cm/s both PCR amplitude and phase become approximately independent of the front surface recombination velocity. This is because the effect of the surface recombination on the PCR signal is still negligible at the low-rate end and is fully developed and saturated at the high-rate end [10].

The effect of the back surface recombination velocity on the PCR signal is still negligible at the low-rate end and is fully developed and saturated at the high-rate end. The reasons for this effect are explained in the Refs. [7,10,11].

According to the above analysis the PCR technique can be used for the characterization of semiconductor samples by means of determining simultaneously the transport parameters.

4. Experimental results

The experimental setup used for frequency scans and radiometric images for *n*-type silicon wafers with different resistivity values is shown in Fig. 3.

A laser (COHERENT model Compass 415 M), with a wavelength of 532 nm, spotsize of 40 μm and power of 25 mW, is used as the excitation source. The excitation beam was modulated in the range from 10 Hz to 100 kHz via an acoustic-optic modulator (ISOMET model 232-A). The infrared emission was collected by two off-axis paraboloidal mirrors and was focused onto an infrared detector. Infrared PCR measurements utilize an InGaAs detector (THORLABS model PDA 400) with spectral response in the 0.8–1.8 μm range; the radius of the detector is 40 μm. The amplitude and phase signals were sent to a lock-in amplifier (Stanford Research System model SR 830) by a general purpose interface bus (GPIB interface), and processed by a personal computer.

Four *n*-type silicon wafers (Mittel, Bromont-Ontario, Canada) grown from Czochralski ingots, 4 in in diameter (labeled Wafer

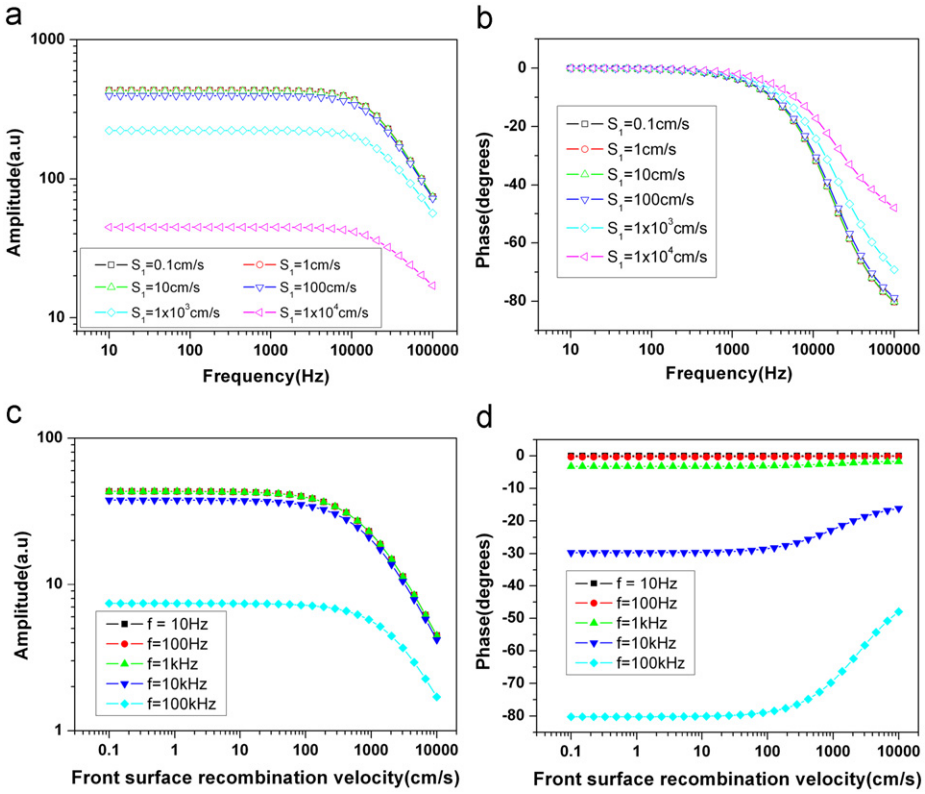

Fig. 2. Simulated PCR signal as a function of the modulation frequency and the front surface recombination velocity. ((a) and (b) correspond to the amplitude and phase of the PCR signal as a function of modulation frequency with the front surface recombination velocity as a parameter. (c) and (d) show the amplitude and phase of the PCR signal as a function of the front surface recombination velocity with the modulation frequency as a parameter).

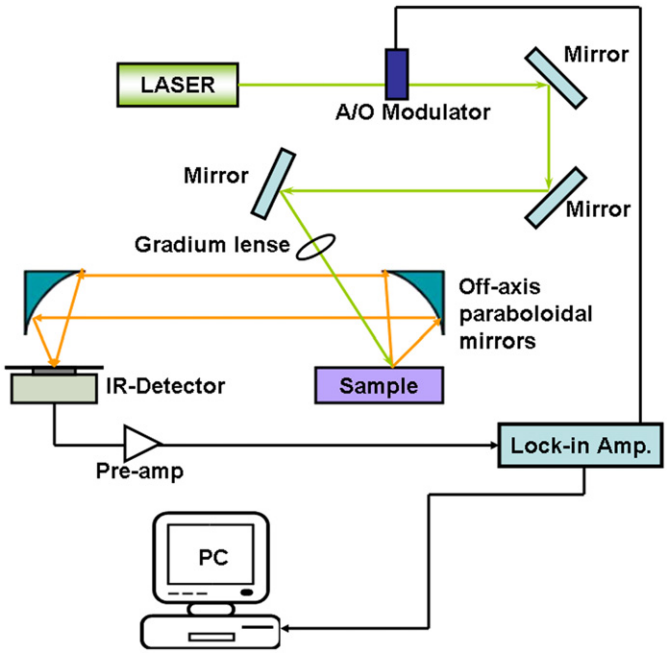

Fig. 3. Schematic diagram of the photocarrier radiometric setup.

No. 1, Wafer No. 2, Wafer No. 3, and Wafer No. 4), and (1 0 0) crystallographic orientation were investigated. In Table 2 are the resistivity and thickness values of the four wafers.

To determine the transport properties of the silicon wafers studied in this work the PCR signal was measured as a function of the modulation frequency in the frequencies range from 10 Hz to 100 kHz . The amplitude and phase of the signal were recorded at a total 30 frequency points spanning from 10 Hz to 100 kHz. Thirteen points on the front surface of the wafers were measured. The points labeled as P1–P7 denote the horizontal direction, while the points labeled as P8–P13 denote the vertical direction, and the point P4 refers to the center of the wafer.

Table 2
Resistivity and thickness values for the *n*-type silicon wafers studied.

Sample	Resistivity (Ω cm)	Thickness (μm)
Wafer No. 1	1–5	523
Wafer No. 2	5–10	517
Wafer No. 3	10–15	530
Wafer No. 4	15–20	516

The experimental data were then fitted to the theoretical model described previously; nevertheless, for simplicity the back surface recombination velocity is set infinite, so the coefficients A_2 and b_2 in the Eq. (6) are taken as $\cong -1$. In the multiparameter fitting procedure, a mean square variance defined as [10]

$$Var = \frac{\sum_{i=1}^{N}\left(1-\frac{A_T(f_i)}{A_E(f_i)}\right)^2}{N} + \frac{\sum_{i=1}^{N}(\Phi_T(f_i)-\Phi_E(f_i))^2}{\sum_{i=1}^{N}(\Phi_E(f_i))^2} \quad (8)$$

is minimized via a least-squares procedure. Here $A_T(f_i)$ and $\Phi_T(f_i)$ are the theoretical amplitude and phase signals, respectively, and $A_E(f_i)$ and $\Phi_E(f_i)$ are the experimental amplitude and phase at modulation frequency f_i, respectively. N is the total number of data points. In the fitting procedure of PCR signal the free parameters were: the carrier lifetime (τ), the carrier diffusion coefficient (D), and the front surface recombination velocity (S_1).

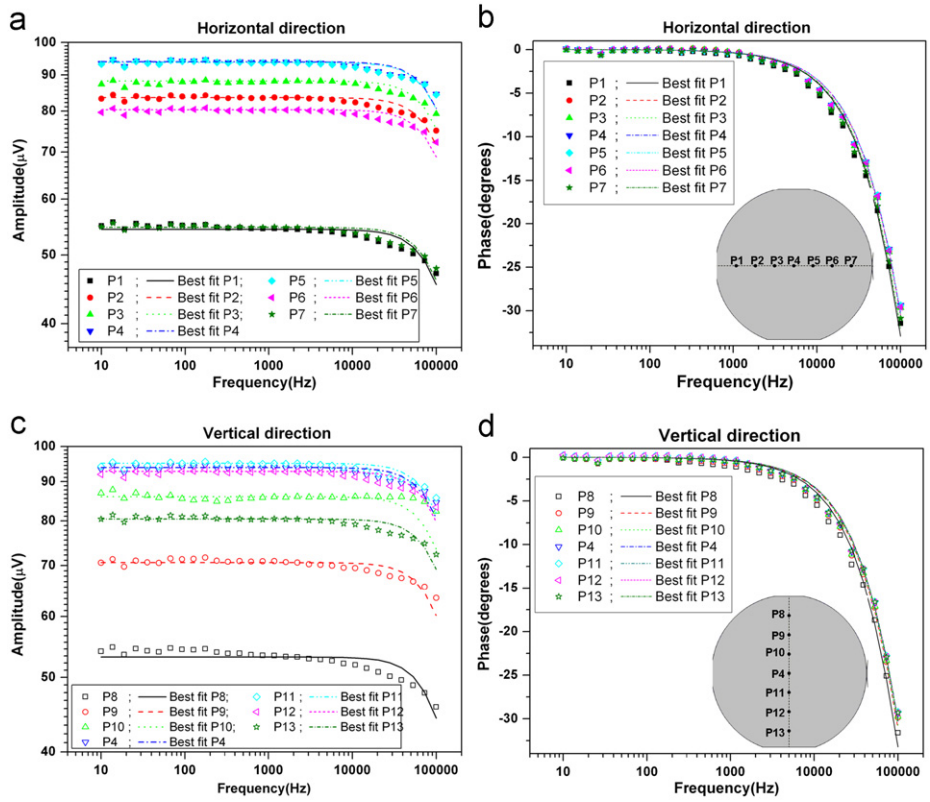

Fig. 4. PCR amplitude and phase frequency scans of thirteen points located on the front surface of Wafer No. 1. (a) and (b) correspond to the horizontal direction (see inset); (c) and (d) correspond to the vertical direction (see inset). The symbols indicate the experimental points, whereas the continuous lines indicate the best theoretical fit.

Table 3
Electronic transport parameters for the Wafer No. 1 determined by a 3D PCR model and the multiparameter best-fit.

	τ (μs)	D (cm^2/s)	S_1 (cm/s)	Error (%)
P1	1.10	15.15	345.54	6
P2	1.01	14.33	465.45	5
P3	1.02	14.33	466.74	5
P4	1.00	14.34	465.27	5
P5	1.00	14.32	465.25	5
P6	1.01	14.33	465.45	5
P7	1.08	14.33	469.31	5
P8	1.11	15.11	346.86	7
P9	1.03	14.35	467.74	6
P10	1.02	14.34	466.82	5
P11	0.99	14.34	464.96	5
P12	1.00	14.34	465.53	5
P13	1.00	14.34	465.55	5

Table 4
Electronic transport parameters for the Wafer No. 2 determined by a 3D PCR model and the best multiparameter fit procedure.

	τ (μs)	D (cm^2/s)	S_1 (cm/s)	Error (%)
P1	1.35	14.57	346.70	5
P2	1.41	14.29	347.42	5
P3	1.30	14.52	341.24	5
P4	1.30	14.80	338.40	5
P5	1.31	14.56	342.07	5
P6	1.42	13.99	356.95	6
P7	1.36	14.72	345.61	6
P8	1.35	14.61	349.53	5
P9	1.35	14.61	349.53	5
P10	1.34	14.64	343.14	5
P11	1.35	14.65	339.61	5
P12	1.35	14.64	339.89	5
P13	1.35	14.65	339.61	5

The experimental data and the corresponding best fits for the Wafer No. 1 are presented in Fig. 4. The lines in these figures represent the best fits, while the symbols are related to the data. The fitted results are shown in Table 3 and the corresponding errors are in the last column of the table. The PCR measurements (not shown here) for the other wafers, Wafer No. 2–4, were similar to those for Wafer No. 1: the points near to the central region of each one of the wafers have similar photoelectronic properties; this fact can be attributed to the industrial growth process of wafers of great size. The parameters of these wafers are summarized in Tables 4–6. Variations in the recombination lifetime over silicon wafers were observed in as-grown Czochralski high-resistivity wafers [12] and can be attributed to both variations in Shockley-Read centers and in variations in majority-carrier concentration as evidenced by variations in the dc free-carrier absorption coefficient. However, when averaging the time obtained for the different points near to the central region of each one wafer it is observed that apparently the higher resistivity wafers have longer lifetimes. This result agrees with the results obtained by Rodríguez et al. [7] in the characterization of *p*-type silicon wafers using the photothermal radiometry technique; although, it is necessary to work further in order to try to establish a correlation between lifetime and nominal resistivity of the wafers. Fig. 5 shows the wafers mean lifetime versus the nominal resistivity; in the inset the recombination lifetime versus carrier concentration is plotted. These results agree with the results previously obtained by Polla [12].

4.1. Photoelectronic images

According to the simulations of the lifetime recombination for the PCR signal (see Fig. 1), the experimental curves (see Fig. 4) and

Table 5
Electronic transport parameters for the Wafer No. 3 determined by a 3D PCR model and the best multiparameter fit procedure.

	τ (μs)	D (cm^2/s)	S_1 (cm/s)	Error (%)
P1	1.42	14.27	348.08	6
P2	1.41	14.29	347.78	6
P3	1.42	14.26	348.16	7
P4	1.48	16.16	460.06	8
P5	1.42	14.26	348.19	7
P6	1.48	16.15	460.35	8
P7	1.43	14.64	334.05	6
P8	1.42	14.26	348.16	6
P9	1.40	14.30	348.20	6
P10	1.45	16.09	449.66	7
P11	1.42	14.26	348.22	7
P12	1.43	14.64	333.93	8
P13	1.55	16.44	452.03	8

Table 6
Electronic transport parameters for the Wafer No. 4 determined by a 3D PCR model and the best multiparameter fit procedure.

	τ (μs)	D (cm^2/s)	S_1 (cm/s)	Error (%)
P1	1.47	16.11	460.72	4
P2	16.28	29.39	1422.95	2
P3	1.89	18.21	383.03	6
P4	0.91	14.29	459.65	2
P5	2.62	15.72	256.34	7
P6	15.85	39.50	0.68	5
P7	38.58	43.42	1.16	9
P9	3.84	4.39	338.22	9
P10	4.00	0.27	365.48	4
P11	1.70	15.74	434.94	7
P12	2.05	15.92	290.71	7

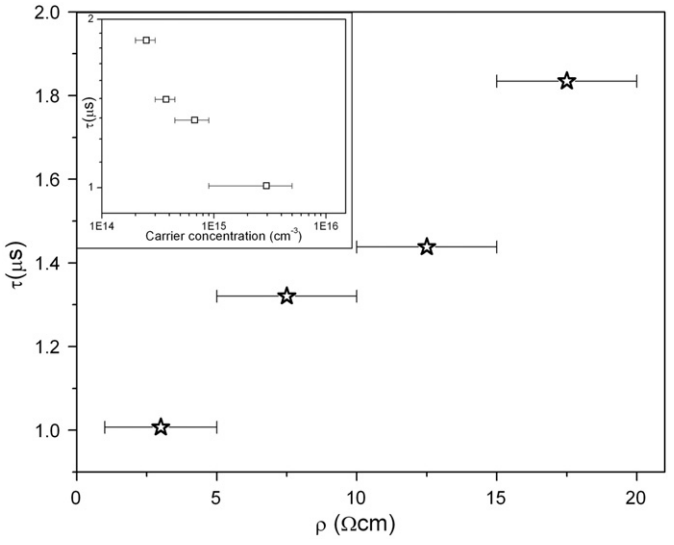

Fig. 5. Mean recombination lifetime of the wafers versus the nominal resistivity of the wafers. In the inset the recombination lifetime of the wafers versus carrier concentration is plotted.

previous publications [8,13] there is a relation between the recombination lifetime and the amplitude and phase. Thus, photoelectronic images can be generated taking the radiometric signal over different points on the sample maintaining the modulation frequency at a fixed value and these images are related directly with the carrier lifetime. The photoelectronic images were measured moving two micrometric screws in x–y directions of a XY stage where the sample was placed; in addition, the modulation frequency was fixed to 10 kHz.

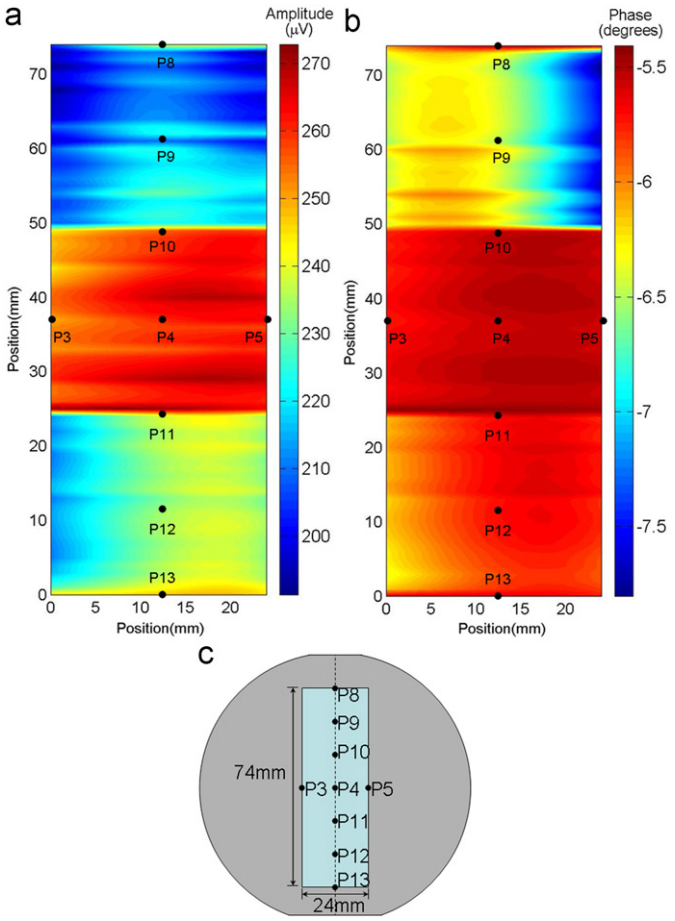

Fig. 6. PCR images of Wafer No. 1 scanned on the front surface of the wafer ((a) amplitude and (b) phase). (c) shows the location of the scanned points on the surface on the wafer.

Fig. 6 shows the PCR images (amplitude and phase) of the front surface of Wafer No. 1. The scan area was of 24 mm × 74 mm and contains the points P3–P5, and P8–P13 in which the frequency scans corresponding to frequency scan were performed (see Fig. 4).

The images above show that the wafer is not photoelectronically homogeneous. The contrast differences observed in the amplitude image are related to the changes in the absorption coefficient, the reflectivity, the recombination lifetime and surface effects such as the variations in the front surface recombination and the surface damage [14]. On the other hand, the contrast variations in the phase image are mainly connected to the variations in the recombination lifetime; besides, the phase is independent of the surface optical effects and the variations in the absorption coefficient and reflectivity. Consequently, the phase image is the true carrier-wave image.

For the other wafers the photoelectronic images are similar (not shown here) and apparently a correlation exists between the nominal resistivity and recombination lifetime according to the results of the Tables 3–6 and Fig. 5.

Taking into account that the PCR images are related with the recombination lifetime the photocarrier radiometry technique has been applied to examine photoelectronically the surface of a porous silicon sample. Fig. 7 shows the PCR images of a porous silicon sample obtained for the first time. This porous sample was produced by electrochemical etching of (1 0 0) n-type silicon

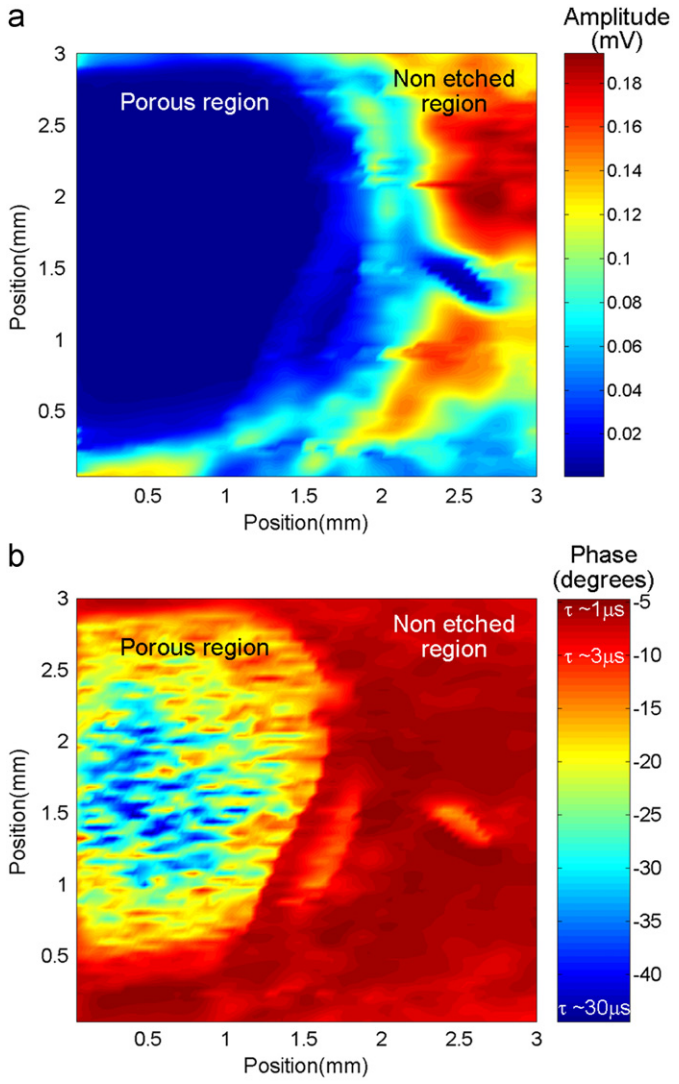

Fig. 7. PCR images of a porous silicon sample ((a) amplitude and (b) phase) (for interpretation of the references to color in this figure, the reader is referred to the web version of this article).

Wafer No. 2 with nominal resistivity value equal to 5–10 Ωcm at room temperature in an electrolytic etching bath of 1:1 mixture of hydrofluoric acid (HF 48 wt%) and ethanol (96 wt%) under a constant voltage (20 V) and etching time of 2 min [15,16]. The images correspond to an area of 3 mm × 3 mm where the interface between porous region and non porous region is presented; for taking these images the modulation frequency of the laser intensity was fixed to 10 kHz, the step was 40 μm and the laser beam diameter was 40 μm. The diverse color on images represents different minority carrier lifetime in the regions. The porous region can be identified at positions where the amplitude (Fig. 7a) is in the range ~0.01–0.05 mV and the phase in the range from ~−10° to −45° (this region is among the red and blue colors of the Fig. 7b, and corresponds to the label "porous region"). According to the simulation results of the PCR phase signal (see Fig. 1d) the recombination lifetime in this region is in the range 3–30 μs. The minority carrier lifetime is dependent on crystal imperfections, such as micro-defects or dislocations [17]; as a result, the difference in the minority recombination lifetime observed in Fig. 7b is related to the micro-defects in the sample surface: the pores. Although the pores can be distinguished (blue color regions in Fig. 7b), it is not possible to determine their size from the PCR phase image.

5. Conclusions

A three-dimensional theoretical model for the PCR signal was presented. Simulations of the PCR signals as a function of the carrier recombination lifetime and front surface recombination velocity have been performed. The PCR technique has been used to characterize *n*-type silicon wafers. The results of the carrier recombination lifetime for the four *n*-type silicon wafers with different resistivity values show that there is a relation between this transport parameter and the nominal resistivity: higher resistivity wafers have longer lifetimes. A more detailed study is necessary, however. By means of photoelectronic images it is possible to "see" the surface state of a silicon wafer.

For the first time photoelectronic images of a porous silicon sample were obtained.

Acknowledgments

This work was partially supported by COLCIENCIAS (Colombia), DINAIN-Universidad Nacional de Colombia (Colombia), and UNAM (México). A.G. wishes to thank support by COLCIENCIAS (Colombia) and Dirección Nacional de Investigación DINAIN, Universidad Nacional de Colombia (Colombia) (Programa Créditos Condonables para Doctorados Nacionales 2004) for her Ph.D. studies.

References

[1] A. Mandelis, J. Batista, D. Shaughnessy, Phys. Rev. B 67 (2003) 205208.
[2] B. Li, D. Shaughnessy, A. Mandelis, J. Batista, J. Garcia, J. Appl. Phys. 95 (2004) 7832.
[3] R. Velázquez-Hernández, J. García-Rivera, M.E. Rodriguez Garcia, S. Jimenez Sandoval, J.G. Mendoza-Alvarez, J.A. Garcia, J. Appl. Phys. 101 (2007) 023105.
[4] A. Mandelis, Diffusion-Wave Fields: Mathematical Methods and Green Functions, Springer, New York, 2001 (Chapter 9).
[5] T. Ikari, A. Salnick, A. Mandelis, J. Appl. Phys. 85 (1999) 7392.
[6] D.F. Edwards, in: E.D. Palik (Ed.), Handbook of Optical Constants of Solids, Academic, New York, 1998.
[7] M.E. Rodríguez, A. Mandelis, L. Nicolaides, J. García, J. Riopel, J. Electrochem. Soc. 147 (2000) 687.
[8] W.H. Press, Numerical Recipes in Fortran 77: The Art of Scientific Computing, Cambridge University Press, 1997.
[9] D. Shaughnessy, A. Mandelis, J. Appl. Phys. 93 (2003) 5244.
[10] B. Li, D. Shaughnessy, A. Mandelis, J. Appl. Phys. 97 (2005) 023701.
[11] D. Shaughnessy, A. Mandelis, J. Appl. Phys. 93 (2003) 5236.
[12] D.L. Polla, IEEE Electron Dev. Lett. EDL-4 (1983) 185.
[13] A. Mandelis, NDT & E Int. 39 (2006) 244.
[14] B. Li, D. Shaughnessy, A. Mandelis, J. Batista, J. García, J. Appl. Phys. 96 (2004) 186.
[15] A. Gutiérrez, Production and Characterization of Porous Silicon Applying Photothermal Techniques, Ph.D. Thesis, Universidad Nacional de Colombia, Bogotá, DC, Colombia, 2009.
[16] A. Gutiérrez, J. Giraldo, R. Velázquez-Hernández, M.L. Mendoza-López, D.G. Espinosa-Arbeláez, A. Del Real, M.E. Rodríguez-García, Rev. Sci. Instrum. 81 (2010) 013901.
[17] Y. Zhao, D. Li, J. Zhao, W. Sang, D. Yang, M. Jiang, Curr. Appl. Phys. 8 (2008) 206.